Postural instability recruits shorter-timescale processes into the non-Gaussian cascade processes

Mariusz, P. Furmanek[a,b], Madhur Mangalam[a,*], Damian G. Kelty-Stephen[c], and Grzegorz Juras[b]

[a]Department of Physical Therapy, Movement and Rehabilitation Sciences, Northeastern University, Boston, MA 02115, USA

[b]Institute of Sport Sciences, The Jerzy Kukuczka Academy of Physical Education, 40-065 Katowice, Poland

[c]Department of Psychology, Grinnell College, Grinnell, IA 50112, USA

[*]Corresponding author at: Department of Physical Therapy, Movement and Rehabilitation Sciences, Northeastern University, Boston, MA 02115, USA.

E-mail addresses: m.furmanek@northeastern.edu (M. P. Furmanek); m.mangalam@northeastern.edu (M. Mangalam).

Abstract

Healthy human postural sway exhibits strong intermittency, reflecting a richly interactive foundation of postural control. From a linear perspective, intermittent fluctuations might be interpreted as engagement and disengagement of complementary control processes at distinct timescales or from a nonlinear perspective, as cascade-like interactions across many timescales at once. The diverse control processes entailed by cascade-like multiplicative dynamics suggest specific non-Gaussian distributional properties at different timescales. Multiscale probability density function (PDF) analysis showed that when standing quietly, stable sand-filled loading of the upper extremities would elicit non-Gaussianity profiles showing a negative-quadratic crossover between short and long timescales. Unstable water-filled loading of the upper extremities would elicit simpler monotonic decreases in non-Gaussianity, that is, a positive-quadratic cancellation of the negative-quadratic crossover. Multiple known indices of postural sway governed the appearance or disappearance of the crossover. Finally, both loading conditions elicited Lévy-like distributions over progressively larger timescales. These results provide evidence that postural instability recruits shorter-timescale processes into the non-Gaussian cascade processes, that indices of postural sway moderate this recruitment, and that postural control under unstable loading shows stronger statistical hallmarks of cascade structure.

Keywords: center of pressure; inverse power law; Lévy walk; postural control; quite stance; scale invariance

1. Introduction

The human body shows strong intermittent fluctuations as it continually sways about a constant fixed position of the global ground reaction force (center of pressure, CoP). Within the center of the base of support, postural sway entails the so-called open-loop control proceeding unchecked. As the body tilts towards the margin of the base of support, postural sway follows the so-called closed-loop control to generate postural corrections based on sensory feedback [1,2]. These corrections embody cascade-like interactions across multiple timescales that include active mechanical processes [3–5], passive reflex mechanisms [6,7] anticipatory [8–10] and feedback processes [11–13], and exploratory processes used by the central nervous system (CNS) to generate sensory information [14,15], which integrate information from visual, vestibular, and somatosensory receptors, in conjunction with the passive properties of the musculoskeletal system. Crucially, we can manipulate the dynamics of these processes by burdening posture with an unstable load on the shoulders. This study aims to demonstrate that unstable loading of the upper arms can recruit this cascade of postural corrections into the short-scales traditionally associated with open-loop control.

Intermittency in postural sway due to cascade-like interactions should entail characteristic signatures on the distributional properties of sway at specific timescales. Indeed, at shorter timescales, sway resembles Brownian motion [1,2], exhibiting strong temporal correlations across steps drawn from thin-tailed distributions with finite-variance (e.g., exponential) [16]. In contrast, at longer timescales, sway reflects weak temporal correlations across steps drawn from non-Gaussian distributions reflecting cascade-like corrections [17]. These distributions can be 'Lévy-like,' with heavy scale-invariant tails potentially tempered with finite variance (e.g., lognormal) or untempered Lévy-stable with infinite variance [18]. Notably, the PDF-tail heaviness bears an inverse relationship with temporal correlations [19,20]. Given that the Lévy-like distributions of sway at longer timescales reflect postural corrections, the stability demands of the task must influence the timescale-dependency of distributional properties of sway.

The signature of intermittency is the growth of variance beyond Gaussian bounds over a wide range of scales. Multiscale PDF analysis can quantify intermittency in turbulent fluid flow through a metric λ_s^2 [21]. Whereas standard distribution-fitting via maximum likelihood estimation (MLE) is more sensitive to the more poorly populated tail, multiscale PDF analysis achieves more robust results by fitting the distribution's better-populated center. For cascade-type multiplicative processes, λ_s^2 decreases monotonically with the natural logarithm of timescale. Besides quantifying changes in multiscale non-Gaussianity in heart-rate variability (HRV) due to pathology [22–26] and neuronal interspike intervals (ISI) with sleep/wake cycles [27], multiscale PDF analysis also reveals the spread of cascade-like postural corrections from longer to relatively short timescales when standing quietly on less stable surfaces. Just as quiet standing on stable surfaces exhibits a crossover in temporal correlations from short to long timescales [28,29], there is a similar crossover in non-Gaussianity in postural sway [30]. Manipulating the surface of the support to make posture less stable removes this crossover. Specifically, it elicits higher non-Gaussianity in postural sway at shorter timescales and stronger resemblance to the simple monotonic decrease of λ_s^2 with logarithmic timescale. Furthermore, indices of postural sway moderate the strength or weakness of the crossover. So, exogenous surface stability interacts with endogenous postural control to define the non-Gaussianity of CoP.

The present study seeks to clarify the appropriate scope of this interaction between exogenous factors and endogenous postural control. One way to interpret the effect of postural instability on non-Gaussianity is to suppose that non-Gaussianity might be specific to variability in the lower extremities. For instance, non-Gaussianity might be particular to the endogenous control by synergies in the legs. However, an alternative approach is to interpret non-Gaussianity as a function of organism-scale coordinations through the connective-tissue networks spanning the entire body [31,32]. Hence, the present study manipulates stability through an unstable load on the upper arms. Furthermore, to respect the fact that non-Gaussian signatures of cascade dynamics appeared earliest in hydrodynamic research [21], we propose that loading the upper extremities with an unstable water-filled tube will be particularly apt to elicit cascade dynamics in postural control.

We applied multiscale PDF method to study postural control in a tube-balancing task to test three specific hypotheses. We asked participants to stand quietly while bimanually balancing stand-filled and water-filled tubes with lower and higher stability demands, respectively. We reasoned that balancing a water-filled tube would require higher stability to counter the sway due to water movement inside the tube. We predicted that, while relatively stable sand-filled loading of the upper extremities would elicit non-Gaussianity profiles showing a negative-quadratic crossover between short and long timescales (Hypothesis 1a), unstable water-filled loading of the upper extremities would elicit simpler monotonic decreases in non-Gaussianity, that is, a positive-quadratic cancellation of the negative-quadratic crossover (Hypothesis 1b). We also predicted that known indices of postural sway would significantly moderate the quadratic polynomial (Hypothesis 2). We also generally predicted that MLE distribution-fitting in both loading conditions would show Lévy-like distributions over progressively larger timescales (Hypothesis 3).

2. Methods

2.1. Participants

Ten adult men (*mean*±1*SD* age = 21.4±1.1 years) with no neurological, muscular, or orthopedic conditions participated after providing institutionally-approved informed consent.

2.2. Experimental setup and procedure

Sand- and water-filled tubes ($l \times d$ = 150×20 cm, m = 8 kg) loaded the participants' upper extremities as they stood quietly with their feet shoulder-width apart (Fig. 1). The participants completed five 30-s trials per loading condition. The order of the trials was pseudo-randomized across participants. A force platform (AMTI Inc., Watertown, MA) recorded ground reaction forces at 100 Hz for the entire 30 s duration.

2.3. Data processing

All data processing was performed in MATLAB 2019b (Matlab Inc., Natick, MA). Trial-by-trial ground reaction forces yielded a 2D foot center of pressure (CoP) series, each dimension describing CoP position along anterior-posterior (AP) and medial-lateral (ML) axes. Each 30-s trial yielded 3000-sample 2D CoP series and 2999-sample 2D CoP displacement series. Finally, a 1D CoP planar Euclidean displacement (PED) series described postural sway along the transverse plane of the body. Iterated Amplitude Adjusted Fourier Transformation (IAAFT) provided phase-randomized surrogates using original series' spectral amplitudes to preserve only linear temporal correlations [33,34].

2.4. Canonical indices of postural sway

Three linear indices were computed for each CoP PED series: (i) Mean of all fluctuations (CoP_PED_*Mean*), (ii) Standard deviation (CoP_PED_*SD*), and (iii) Root mean square (CoP_PED_*RMSE*).

Four nonlinear indices were computed for each CoP PED series: (i) Sample entropy (CoP_PED_*SampEn*), indexing the extent of complexity in the signal [35]. We used m = 2 and r = 0.2 for computing the *SampEn* [cf. 34]. (ii) Multiscale sample entropy (CoP_PED_*MSE*), indexing signal complexity over multiple timescales [37]. We used m = 2, r = 0.2, and τ = 20 for computing the *MSE* [cf. 34]. (iii) We used detrended fluctuation analysis [38] to compute Hurst's exponent, H_{fGn}, indexing temporal correlations in original CoP PED series (CoP_PED_$H_{\mathrm{fGn_Original}}$) and shuffled versions of each series (CoP_PED_$H_{\mathrm{fGn_Shuffled}}$) using the scaling region: 4, 8, 12,… 1024 [cf. 37]. Shuffling destroys the temporal structure of a signal. (iv) Multifractal spectrum width, $\Delta\alpha$, indexing the extent of multifractal temporal correlations in the signal. Chhabra and Jensen's direct method [40] was used to compute $\Delta\alpha$ for the original CoP series (CoP_PED_$\Delta\alpha_{\mathrm{Original}}$) and the IAAFT surrogate (CoP_PED_$\Delta\alpha_{\mathrm{Surrogate}}$) [cf. 38].

2.5. Multiscale probability density function (PDF) analysis

Multiscale PDF analysis characterizes the distribution of abrupt changes in CoP PED series { $b(t)$ } using the PDF tail. The first step is to generate { $B(t)$ } by integrating { $b(t)$ } after centering by the mean b_{ave} (Fig. 2, top):

$$B(t)=\sum_{i=1}^{t/\Delta t} b(i\Delta t)-b_{ave} \quad .$$

A a 3rd order polynomial detrends { $B(t)$ } within k overlapping windows of length $2s$, s being the timescale (Fig. 2, middle). Intermittent deviation $\Delta_s B(t)$ in k^{th} window from $1+s(k-1)$ to sk in the detrended time series { $B^d(t)=B(t)-f_{fit}(t)$ } is computed as $\Delta_s B^d(t)=B^d(t+s)-B^d(t)$, where $1+s(k-1)\leq t\leq sk$ and $f_{fit}(t)$ is the polynomial representing the local trend of { $B(t)$ }, of which the elimination assures the zero-mean probability density function in the next step (Fig. 2, bottom). Finally, $\Delta_s B$ is normalized by the SD (i.e., variance is set to one) to quantify the PDF.

To quantify the non-Gaussianity of $\Delta_s B$ at timescale s, the standardized PDF constructed from all the $\Delta_s B(t)$ values is approximated by the Castaing model,[21] with λ_s as a single parameter characterizing the non-Gaussianity of the PDF. λ_s is estimated as

$$\lambda_s^2=\frac{2}{q(q-2)}[\ln(\sqrt{\pi}\langle|\Delta_s B|^q\rangle)+\ln\Gamma(\frac{q+1}{2})-\frac{q}{2}\ln 2] \quad ,$$

where $\langle|\Delta_s B|^q\rangle$ denotes an estimated value of qth order absolute moment of { $\Delta_s B$ }. As λ_s^2 increases, the PDF becomes increasingly peaked and fat-tailed (Fig. 3, left). λ_s^2 can be estimated by Eq. (7) based on q^{th} order absolute moment of a time series independent of q. Estimating λ_s^2 based on 0.2th moment (q = 0.2) emphasizes the center part of the PDF, reducing the effects of extreme deviations due to heavy-tails and kurtosis. We used 0.2th moment because estimates of λ_s^2 for a time series of 6000 are more accurate at lower values of q [42].

Cascade-type multiplicative processes yield the inverse relationship λ_s^2 ~ –log s (Fig. 3, right) [24]. For the present purposes, we quantified λ_s^2 for each original CoP PED

series and corresponding IAAFT surrogate at timescales 5 to 1000 samples (i.e., 50 ms to 10 s) at steps of 5 samples (50 ms).

To test explicitly for Levy-likeness, we used Akaike Information Criterion (AIC) weights obtained via the more common maximum likelihood estimation (MLE) to determine whether the PDF at each timescale was a power law, lognormal, exponential, or gamma distribution. We include this analysis also to complement multiscale PDF analysis to portray the analytical effect of sensitivity to different portions of the distribution.

2.6. Statistical analysis

To test for crossovers in non-Gaussianity, a linear mixed-effect (LME) model using lmer [43] in R package "lme4" tested λ_s^2 vs. log-timescale curves for orthogonal linear and quadratic polynomials, for interactions with grouping variables (Loading condition×Original, where Original encoded differences in original series from surrogates) and with indices of postural sway (Section 2.4.). Statistical significance was assumed at the alpha level of 0.05 using R package "lmerTest" [44]. To test how lognormality changed with log-timescale, a generalized linear mixed-effect (GLME) fit changes in Lognormality as a dichotomous variable using orthogonal linear, quadratic, and cubic polynomials and tested interaction effects of grouping variables (Loading condition×Original) with those polynomials using glmer [45] in lme4.

3. Results

Figs. 4 provide a schematic of multiscale PDF characterization of postural sway in representative participants balancing sand- and water-filled tubes for 30 s.

3.1. Effects of Loading condition on λ_s^2 vs. log-timescale curves

In the sand-filled condition, λ_s^2 vs. log-timescale curves showed stronger linear decrease (B = –3.30, p < 0.001) and stronger negative quadratic, downward-facing parabolic form (B = –2.50, p < 0.001) for the original CoP PED series than the surrogates (Table S1; Fig. 5, left). Balancing the water-filled tube elicited a significant reversal of this parabolic form (B = 0.50, p < 0.014). Specifically, in the water-filled condition, λ_s^2 vs. log-timescale curves for the original CoP PED series showed both a stronger linear decrease (B = –2.93, p < 0.001) and a further—though only approaching-significant—reversal of the downward-facing parabolic form (B = 0.49, p = 0.094).

The only significant change in the parabolic form of λ_s^2 vs. log-timescale curves depended on the indices of postural sway. That is, the main effect of quadratic relationships between λ_s^2 and log-timescale, the difference in this quadratic form between the original CoP PED series vs. the surrogates, and the difference in this quadratic form due to the water-filled tube for the original COP PED series yielded non-significant coefficients (ps > 0.05; Table S2). The surrogates showed only marginally significant differences between the sand- and water-filled conditions (B = –11.88, p = 0.068).

Otherwise, indices of postural sway contributed to ten significant differences—and four marginally significant differences—in the quadratic form of λ_s^2 vs. log-timescale curves (Table S2). Seven of these effects pertained directly with the strength of the downward-opening parabolic form. Increases in CoP_PED_*RMSE* and CoP_PED_$H_{\text{fGn_Original}}$ accentuated the negative quadratic form in the original COP PED series vs. the surrogates (B = –1.37×10^6

p = 0.032; and B = –14.43, p = 0.053, respectively). Increases in CoP_PED_$H_{\text{fGn_Original–Shuffled}}$ accentuated the negative quadratic form in the water-filled condition (B = –13.68, p = 0.055). Increases in CoP_PED_*Mean*, CoP_PED_*SD*, CoP_PED_*MSE*, and the original-minus-surrogate difference in CoP_PED_H_{fGn} accentuated the negative quadratic form for the original COP PED series vs. the surrogates in the water-filled condition (B = 1.06×10^6 p = 0.037; B = 8.04×10^5, p < 0.038; B = –6.66, p = 0.009; and B = –1.24×10^3, p < 0.074, respectively).

On the other hand, seven of these effects pertained inversely with the strength of the downward-opening parabolic form, effectively reversing the negative quadratic form in the sand-filled condition. Increases in CoP_PED_*Mean*, CoP_PED_*SD*, CoP_PED_*MSE*, and CoP_PED_$\Delta\alpha_{\text{Original–Surrogate}}$ contributed positive quadratic coefficients for the original COP PED series vs. the surrogates (B = 1.09×10^6, p = 0.032; B = 8.28×10^5, p = 0.033; B = 14.49, p < 0.001; and B = 2.73×10^3, p < 0.001, respectively). Increases in CoP_PED_H_{fGn} contributed quadratic coefficients in the water-filled condition (B = 15.35, p = 0.028). Increases in CoP_PED_*RMSE* and CoP_PED_$\Delta\alpha_{\text{Original}}$ contributed positive quadratic coefficients for the original COP PED series vs. the surrogates in the water-filled condition (B = 1.33×10^6, p = 0.037; and B = 1.26×10^3, p = 0.070, respectively).

3.2. Effects of Loading condition on the growth of lognormality in postural sway with log-timescale

The surrogates exhibited significantly less lognormality in the water-filled than the sand-filled condition (B = –0.26, p < 0.001), and the original COP PED series in both the sand- and water-filled conditions exhibited less lognormality (B = –1.83, p < .0001). In the original CoP PED series, lognormality in postural sway increased as a cubic function of log-timescale, with significant positive linear (B = 19.09, p < 0.001) and significant negative cubic forms (B = –71.87, p < 0.001; Table S3; Fig. 5, right). The quadratic component of the lognormality vs. log-timescale relationship was not significant (p > 0.05). In contrast, in the surrogates, the growth of lognormality showed a parabolic form with a significant linear increase and quadratic decrease with log-timescale in the sand-filled condition (B = 53.07, p < 0.001; and B = –34.32, p < 0.001, respectively). These linear and quadratic effects became stronger in the water-filled condition (B = 20.43, p < 0.001; and B = –40.34, p < 0.001, respectively), but crucially, this difference between the sand- and water-filled conditions was the same for the original CoP PED series and the surrogates.

4. Discussion

Multiscale PDF analysis supported Hypothesis 1a that stable sand-filled loading of the upper extremities would elicit quiet standing with non-Gaussianity profiles showing a negative-quadratic crossover between short and long timescales. It also supported Hypothesis 1b that unstable water-filled loading of the upper extremities would elicit simpler monotonic decreases in non-Gaussianity, that is, a positive-quadratic cancellation of the negative-quadratic crossover. Indices of postural sway governed the appearance or disappearance of the crossover, thus supporting Hypothesis 2. Finally, supporting Hypothesis 3, both loading conditions elicited Lévy-like distributions over progressively larger timescales, confirming the cascade structure of postural control and the stronger sensitivity of multiscale PDF analysis to non-Gaussianity. These results provide evidence that postural instability recruits shorter-timescale processes into the non-Gaussian cascade processes, that indices of postural sway moderate this recruitment, and that postural control under unstable loading

shows stronger statistical hallmarks of cascade structure, strengthening evidence of cascade processes in postural control.

A noteworthy finding of the present study is that postural sway reflects two competing processes amenable to the task's stability demands. Higher potential of heavy-tailed fluctuations at sufficiently longer timescales, as indicated by the change in PDF from exponential to lognormal at these longer timescales, indicate definite postural adjustments. Unstable water-filled loading of the upper extremities was associated with a higher non-Gaussianity as well as a higher potential of heavy-tailed fluctuations at shorter timescales than stable sand-filled loading of the upper extremities, indicating that both these processes can be selectively recruited at shorter timescales.

The present study open a new lens on the flexible interactive foundation of postural control. Non-Gaussianity confirmed by a new analytical method means a lot for the growing appreciation of the cascade structure in postural control. The cascade structure supporting postural control is no airy mathematical abstraction unmoored from the physiological details. Instead, we can pinpoint the physiological substance: the vast network of connective tissues and extracellular matrix (ECM) that has been imagined as a multifractal tensegrity (MFT) in which the components hang together under tensional and compressional forces at multiple scales [31,32,46–51]. This network cooperates directly and uninterruptedly with the nervous system and exhibits similar cascade-like structure as found in "neuronal avalanches" [52]. It can be no small coincidence that tensegrity and avalanche models all converge on the same multifractal geometry [53,54] that inspired the development of multiscale PDF quantification of non-Gaussianity [22,24,55]. Hence, this bodywide aspect suggests multiple points of entry through which stimulation can elicit cascade processes to spread from longer to shorter timescales—from the surface underfoot [30] and now from the loads at hand. Crucially, the empirical estimates of multifractal structure along this physiological cascade well predict the flow of perceptual information through the body and toward the coordination of disparate body parts [39,41,56,57]. A challenge for future work is to characterize how task- and age-specific changes these connective and neural tissues impact their interweaving in the bodywide cascade.

Supplementary material

Table S1. Coefficients of linear mixed-effect (LME) model examining the effect of Loading condition on λ_s^2 vs. log-timescale curves.

Table S2. Coefficients of LME model examining the effects of Loading condition on λ_s^2 vs. log-timescale curves for orthogonal linear and quadratic polynomials, for interactions with indices of postural sway.

Table S3. Coefficients of generalized linear mixed-effect (GLME) model examining the effect of Loading condition on the growth of lognormality in postural sway with log-timescale.

Author contributions

M.P.F. and M.M. conceived and designed research; M.M. and D.G.K-S. analyzed data; M.P.F., M.M, and D.G.K-S. interpreted results of experiments; M.M. prepared figures; M.M. and D.G.K-S. drafted manuscript; M.P.F., M.M., D.G.K-S., and G.J. edited and revised manuscript; M.P.F., M.M., D.G.K-S., and G.J. approved final version of manuscript.

References

[1] J.J. Collins, C.J. De Luca, Open-loop and closed-loop control of posture: A random-walk analysis of center-of-pressure trajectories, Exp. Brain Res. 95 (1993) 308–318. https://doi.org/10.1007/BF00229788.

[2] J.J. Collins, C.J. De Luca, Upright, correlated random walks: A statistical-biomechanics approach to the human postural control system, Chaos An Interdiscip. J. Nonlinear Sci. 5 (1995) 57–63. https://doi.org/10.1063/1.166086.

[3] D.A. Winter, Human balance and posture control during standing and walking, Gait Posture. 3 (1995) 193–214. https://doi.org/10.1016/0966-6362(96)82849-9.

[4] D.A. Winter, A.E. Patla, M. Ishac, W.H. Gage, Motor mechanisms of balance during quiet standing, J. Electromyogr. Kinesiol. 13 (2003) 49–56. https://doi.org/10.1016/S1050-6411(02)00085-8.

[5] D.A. Winter, A.E. Patla, F. Prince, M. Ishac, K. Gielo-Perczak, Stiffness control of balance in quiet standing, J. Neurophysiol. 80 (1998) 1211–1221. https://doi.org/10.1152/jn.1998.80.3.1211.

[6] R. Fitzpatrick, D. Burke, S.C. Gandevia, Loop gain of reflexes controlling human standing measured with the use of postural and vestibular disturbances, J. Neurophysiol. 76 (1996) 3994–4008. https://doi.org/10.1152/jn.1996.76.6.3994.

[7] A.M. Bacsi, J.G. Colebatch, Evidence for reflex and perceptual vestibular contributions to postural control, Exp. Brain Res. 160 (2005) 22–28. https://doi.org/10.1007/s00221-004-1982-2.

[8] G.N. Gantchev, D.M. Dimitrova, Anticipatory postural adjustments associated with arm movements during balancing on unstable support surface, Int. J. Psychophysiol. 22 (1996) 117–122. https://doi.org/10.1016/0167-8760(96)00016-5.

[9] M. Klous, P. Mikulic, M.L. Latash, Two aspects of feedforward postural control: Anticipatory postural adjustments and anticipatory synergy adjustments, J. Neurophysiol. 105 (2011) 2275–2288. https://doi.org/10.1152/jn.00665.2010.

[10] M. Klous, P. Mikulic, M.L. Latash, Early postural adjustments in preparation to whole-body voluntary sway, J. Electromyogr. Kinesiol. 22 (2012) 110–116. https://doi.org/10.1016/j.jelekin.2011.11.005.

[11] R.J. Peterka, P.J. Loughlin, Dynamic regulation of sensorimotor integration in human postural control, J. Neurophysiol. 91 (2004) 410–423. https://doi.org/10.1152/jn.00516.2003.

[12] R.J. Peterka, Sensorimotor integration in human postural control, J. Neurophysiol. 88 (2002) 1097–1118. https://doi.org/10.1152/jn.2002.88.3.1097.

[13] N. Teasdale, M.P. Furmanek, M. Germain Robitaille, F.C.L. de Oliveira, M. Simoneau, Sensory integration during vibration of postural muscle tendons when pointing to a memorized target, Front. Hum. Neurosci. 10 (2017) 682. https://doi.org/10.3389/fnhum.2016.00682.

[14] M.G. Carpenter, C.D. Murnaghan, J.T. Inglis, Shifting the balance: Evidence of an exploratory role for postural sway, Neuroscience. 171 (2010) 196–204. https://doi.org/10.1016/j.neuroscience.2010.08.030.

[15] C.D. Murnaghan, B.C. Horslen, J.T. Inglis, M.G. Carpenter, Exploratory behavior during stance persists with visual feedback, Neuroscience. 195 (2011) 54–59. https://doi.org/10.1016/j.neuroscience.2011.08.020.

[16] E.A. Codling, M.J. Plank, S. Benhamou, Random walk models in biology, J. R. Soc. Interface. 5 (2008) 813–834. https://doi.org/10.1098/rsif.2008.0014.

[17] N. Kuznetsov, S. Wallot, Effects of accuracy feedback on fractal characteristics of time estimation, Front. Integr. Neurosci. 5 (2011) 62. https://doi.org/10.3389/fnint.2011.00062.

[18] D.W. Sims, E.J. Southall, N.E. Humphries, G.C. Hays, C.J.A. Bradshaw, J.W. Pitchford, A. James, M.Z. Ahmed, A.S. Brierley, M.A. Hindell, D. Morritt, M.K. Musyl, D. Righton, E.L.C. Shepard, V.J. Wearmouth, R.P. Wilson, M.J. Witt, J.D. Metcalfe, Scaling laws of marine predator search behaviour, Nature. 451 (2008) 1098–1102. https://doi.org/10.1038/nature06518.

[19] N. Scafetta, P. Grigolini, Scaling detection in time series: Diffusion entropy analysis, Phys. Rev. E. 66 (2002) 36130. https://doi.org/10.1103/PhysRevE.66.036130.

[20] A.M. Reynolds, Truncated Lévy walks are expected beyond the scale of data collection when correlated random walks embody observed movement patterns, J. R. Soc. Interface. 9 (2012) 528–534. https://doi.org/10.1098/rsif.2011.0363.

[21] B. Castaing, Y. Gagne, E.J. Hopfinger, Velocity probability density functions of high Reynolds number turbulence, Phys. D Nonlinear Phenom. 46 (1990) 177–200. https://doi.org/10.1016/0167-2789(90)90035-N.

[22] K. Kiyono, Z.R. Struzik, N. Aoyagi, S. Sakata, J. Hayano, Y. Yamamoto, Critical scale invariance in a healthy human heart rate, Phys. Rev. Lett. 93 (2004) 178103. https://doi.org/10.1103/PhysRevLett.93.178103.

[23] K. Kiyono, Z.R. Struzik, N. Aoyagi, Y. Yamamoto, Multiscale probability density function analysis: Non-Gaussian and scale-Invariant fluctuations of healthy human heart rate, IEEE Trans. Biomed. Eng. 53 (2006) 95–102. https://doi.org/10.1109/TBME.2005.859804.

[24] K. Kiyono, J. Hayano, E. Watanabe, Z.R. Struzik, Y. Yamamoto, Non-Gaussian heart rate as an independent predictor of mortality in patients with chronic heart failure, Hear. Rhythm. 5 (2008) 261–268. https://doi.org/10.1016/j.hrthm.2007.10.030.

[25] K. Kiyono, J. Hayano, S. Kwak, E. Watanabe, Y. Yamamoto, Non-gaussianity of low frequency heart rate variability and sympathetic activation: Lack of increases in multiple system atrophy and parkinson disease, Front. Physiol. 3 (2012) 34. https://doi.org/10.3389/fphys.2012.00034.

[26] J. Hayano, K. Kiyono, Z. Struzik, Y. Yamamoto, E. Watanabe, P. Stein, L. Watkins, J. Blumenthal, R. Carney, Increased non-Gaussianity of heart rate variability predicts cardiac mortality after an acute myocardial infarction, Front. Physiol. 2 (2011) 65. https://doi.org/10.3389/fphys.2011.00065.

[27] L.A. Safonov, Y. Isomura, S. Kang, Z.R. Struzik, T. Fukai, H. Câteau, Near scale-free dynamics in neural population activity of waking/sleeping rats revealed by multiscale analysis, PLoS One. 5 (2010) e12869. https://doi.org/10.1371/journal.pone.0012869.

[28] P. Federolf, P. Zandiyeh, V. von Tscharner, Time scale dependence of the center of pressure entropy: What characteristics of the neuromuscular postural control system influence stabilographic entropic half-life?, Exp. Brain Res. 233 (2015) 3507–3515. https://doi.org/10.1007/s00221-015-4420-8.

[29] D. Delignières, K. Torre, P.-L. Bernard, Transition from persistent to anti-persistent correlations in postural sway indicates velocity-based control, PLOS Comput. Biol. 7 (2011) e1001089. https://doi.org/10.1371/journal.pcbi.1001089.

[30] M. Mangalam, D.G. Kelty-Stephen, Hypothetical control of postural sway, BioRxiv. (2020) 104760. https://doi.org/10.1101/2020.05.19.104760.

[31] M.T. Turvey, S.T. Fonseca, The medium of haptic perception: A tensegrity hypothesis, J. Mot. Behav. 46 (2014) 143–187. https://doi.org/10.1080/00222895.2013.798252.

[32] M.T. Turvey, Action and perception at the level of synergies, Hum. Mov. Sci. 26 (2007) 657–697. https://doi.org/10.1016/j.humov.2007.04.002.

[33] E.A.F. Ihlen, B. Vereijken, Interaction-dominant dynamics in human cognition: Beyond 1/*f* fluctuation, J. Exp. Psychol. Gen. 139 (2010) 436–463. https://doi.org/10.1037/a0019098.

[34] T. Schreiber, A. Schmitz, Improved surrogate data for nonlinearity tests, Phys. Rev. Lett. 77 (1996) 635–638. https://doi.org/10.1103/PhysRevLett.77.635.

[35] J.S. Richman, J.R. Moorman, Physiological time-series analysis using approximate entropy and sample entropy, Am. J. Physiol. Circ. Physiol. 278 (2000) H2039–H2049. https://doi.org/10.1152/ajpheart.2000.278.6.H2039.

[36] J.-H. Ko, K.M. Newell, Aging and the complexity of center of pressure in static and dynamic postural tasks, Neurosci. Lett. 610 (2016) 104–109. https://doi.org/10.1016/j.neulet.2015.10.069.

[37] M. Costa, A.L. Goldberger, C.-K. Peng, Multiscale entropy analysis of complex physiologic time series, Phys. Rev. Lett. 89 (2002) 68102. https://doi.org/10.1103/PhysRevLett.89.068102.

[38] C.-K. Peng, S. V Buldyrev, S. Havlin, M. Simons, H.E. Stanley, A.L. Goldberger, Mosaic organization of DNA nucleotides, Phys. Rev. E. 49 (1994) 1685–1689. https://doi.org/10.1103/PhysRevE.49.1685.

[39] M. Mangalam, R. Chen, T.R. McHugh, T. Singh, D.G. Kelty-Stephen, Bodywide fluctuations support manual exploration: Fractal fluctuations in posture predict perception of heaviness and length via effortful touch by the hand, Hum. Mov. Sci. 69 (2020) 102543. https://doi.org/10.1016/j.humov.2019.102543.

[40] A. Chhabra, R. V Jensen, Direct determination of the *f*(\alpha) singularity spectrum, Phys. Rev. Lett. 62 (1989) 1327–1330. https://doi.org/10.1103/PhysRevLett.62.1327.

[41] M. Mangalam, D.G. Kelty-Stephen, Multiplicative-cascade dynamics supports whole-body coordination for perception via effortful touch, Hum. Mov. Sci. 70 (2020) 102595. https://doi.org/10.1016/j.humov.2020.102595.

[42] K. Kiyono, Z.R. Struzik, Y. Yamamoto, Estimator of a non-Gaussian parameter in multiplicative log-normal models, Phys. Rev. E. 76 (2007) 41113. https://doi.org/10.1103/PhysRevE.76.041113.

[43] D. Bates, M. Mächler, B. Bolker, S. Walker, Fitting linear mixed-effects models using lme4, ArXiv Prepr. ArXiv1406.5823. (2014). https://doi.org/arXiv:1406.5823.

[44] A. Kuznetsova, P.B. Brockhoff, R.H.B. Christensen, lmerTest package: Tests in linear mixed effects models, J. Stat. Softw. 82 (2017) 1548–7660. https://doi.org//10.18637/jss.v082.i13.

[45] W. Lee, K.J. Grimm, Generalized linear mixed-effects modeling programs in R for binary outcomes, Struct. Equ. Model. A Multidiscip. J. 25 (2018) 824–828. https://doi.org/10.1080/10705511.2018.1500141.

[46] D.E. Ingber, Cellular mechanotransduction: Putting all the pieces together again, FASEB J. 20 (2006) 811–827. https://doi.org/10.1096/fj.05-5424rev.

[47] D.E. Ingber, From cellular mechanotransduction to biologically inspired engineering, Ann. Biomed. Eng. 38 (2010) 1148–1161. https://doi.org/10.1007/s10439-010-9946-0.

[48] D.G. Kelty-Stephen, Multifractal evidence of nonlinear interactions stabilizing posture for phasmids in windy conditions: A reanalysis of insect postural-sway data, PLoS One. 13 (2018) e0202367. https://doi.org/10.1371/journal.pone.0202367.

[49] D.E. Ingber, Tensegrity-based mechanosensing from macro to micro, Prog. Biophys. Mol. Biol. 97 (2008) 163–179. https://doi.org/10.1016/j.pbiomolbio.2008.02.005.

[50] D.E. Ingber, Tensegrity and mechanotransduction, J. Bodyw. Mov. Ther. 12 (2008) 198–200. https://doi.org/10.1016/j.jbmt.2008.04.038.

[51] C.S. Chen, D.E. Ingber, Tensegrity and mechanoregulation: From skeleton to cytoskeleton, Osteoarthr. Cartil. 7 (1999) 81–94. https://doi.org/10.1053/joca.1998.0164.

[52] S.R. Miller, S. Yu, D. Plenz, The scale-invariant, temporal profile of neuronal avalanches in relation to cortical γ–oscillations, Sci. Rep. 9 (2019) 16403. https://doi.org/10.1038/s41598-019-52326-y.

[53] T. Zorick, J. Landers, A. Leuchter, M.A. Mandelkern, EEG multifractal analysis correlates with cognitive testing scores and clinical staging in mild cognitive impairment, J. Clin. Neurosci. (2020). https://doi.org/10.1016/j.jocn.2020.04.003.

[54] A. Das, A. Levina, Critical neuronal models with relaxed timescale separation, Phys. Rev. X. 9 (2019) 21062. https://doi.org/10.1103/PhysRevX.9.021062.

[55] B.J. West, M. Turalska, Hypothetical control of heart rate variability, Front. Physiol. 10 (2019) 1078. https://doi.org/10.3389/fphys.2019.01078.

[56] M. Mangalam, N.S. Carver, D.G. Kelty-Stephen, Global broadcasting of local fractal fluctuations in a bodywide distributed system supports perception via effortful touch, Chaos, Solitons & Fractals. 135 (2020) 109740. https://doi.org/10.1016/j.chaos.2020.109740.

[57] M. Mangalam, N.S. Carver, D.G. Kelty-Stephen, Multifractal signatures of perceptual processing on anatomical sleeves of the human body, BioRxiv. (2020) 091702. https://doi.org/10.1101/2020.05.12.091702.

Fig. 1. Experimental setup and task. Each participant stood quietly while bimanually balancing a sand- or water-filled tube for 30 s.

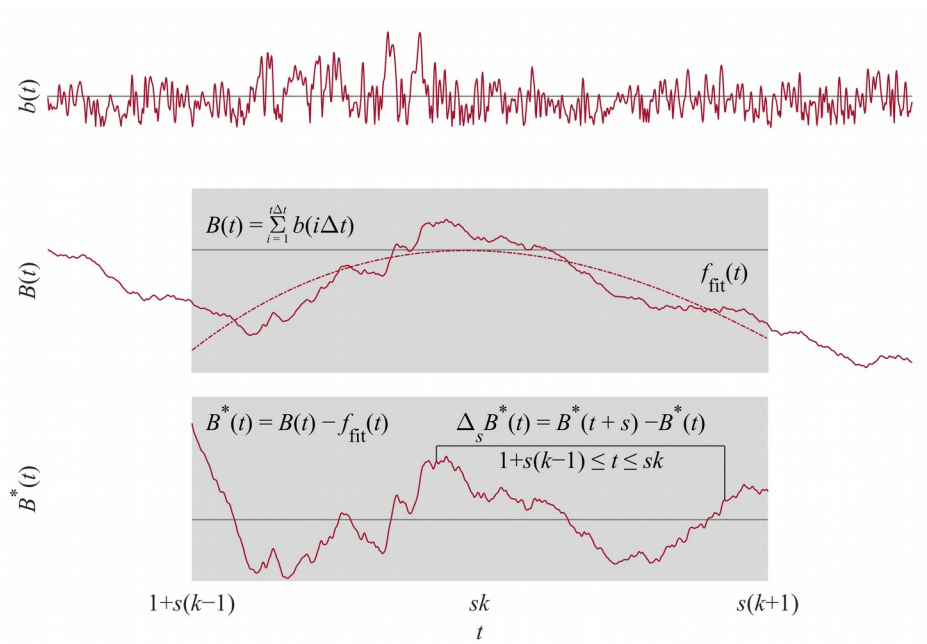

Fig. 2. Schematic illustration of multiscale probability density function (PDF) analysis. Top: The first step is to generate { $B(t)$ } by integrating { $b(t)$ } after centering by the mean b_{ave} : $B(t)=\sum_{i=1}^{t/\Delta t} b(i\Delta t)-b_{ave}$. Middle: A a 3rd order polynomial detrends { $B(t)$ } within k overlapping windows of length $2s$, s being the timescale. Bottom: Intermittent deviation $\Delta_s B(t)$ in k^{th} window from $1+s(k-1)$ to sk in the detrended time series { $B^d(t)=B(t)-f_{fit}(t)$ } is computed as $\Delta_s B^d(t)=B^d(t+s)-B^d(t)$, where $1+s(k-1)\le t\le sk$ and $f_{fit}(t)$ is the polynomial representing the local trend of { $B(t)$ }, of which the elimination assures the zero-mean probability density function in the next step.

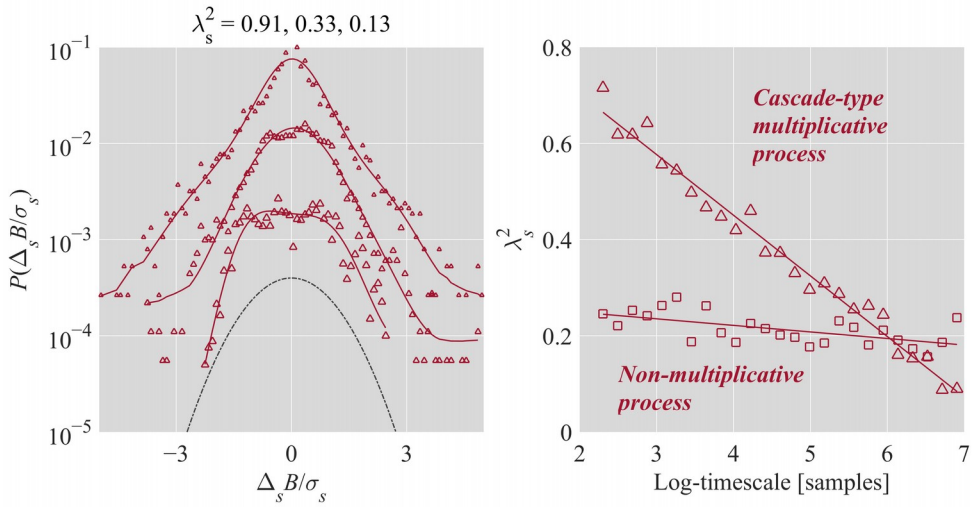

Fig. 3. Schematic illustration of non-Gaussianity index λ_s. Left: The relationship between λ_s^2 and shapes of PDF plotted in linear-log coordinates for λ_s^2 = 0.9, 0.33, and 0.13 (from top to bottom). For clarity, the PDFs have been shifted vertically. As λ_s^2 increases, the PDF becomes increasingly peaked and fat-tailed. As λ_s decreases, the PDF increasingly resembles the Gaussian (dashed line), assuming a perfect Gaussian as λ_s^2 approaches 0. Right: Cascade-type multiplicative processes yield the inverse relationship $\lambda_s^2 \sim -\log s$.

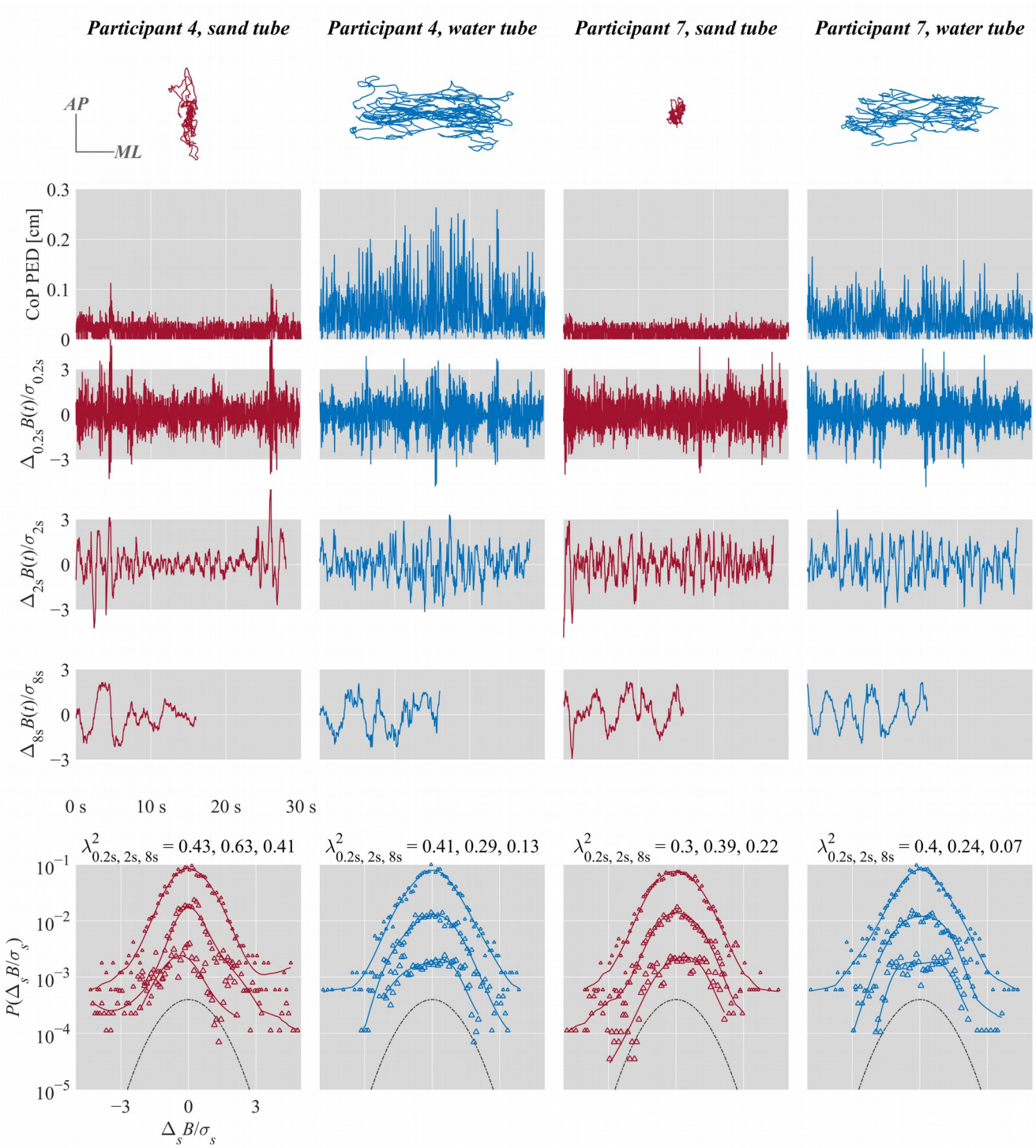

Fig. 4. Multiscale PDF characterization of postural sway in representative participants balancing sand- and water-filled tubes for 30 s. From top to bottom: CoP trajectories along the anterior-posterior (*AP*) and medial-lateral (*ML*) axes. CoP PED series. { $\Delta_s B(i)$ } for s = 0.2, 2, and 8 s. Standardized PDFs (in logarithmic scale) of { $\Delta_s B(i)$ } for s = 0.2, 2, and 8 s (from top to bottom), where σ_s denotes the *SD* of { $\Delta_s B(i)$ }.

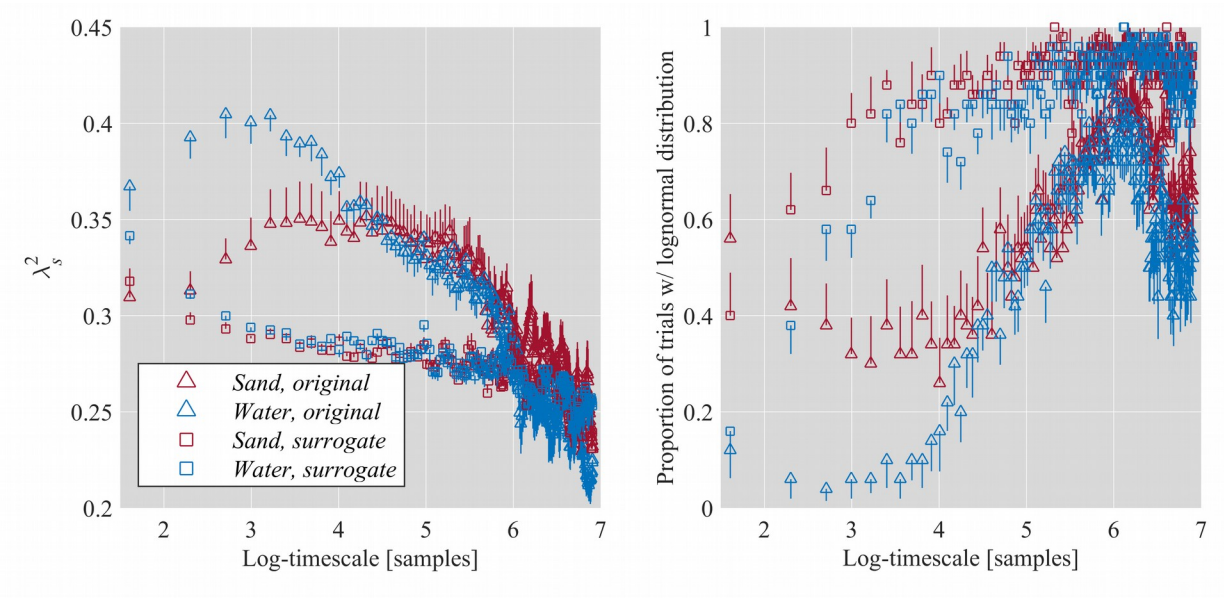

Fig. 5. Log-timescale dependence of mean λ_s^2 (left) and proportion of trials with a lognormal distribution (right), while balancing sand- and water-filled tubes for 30 s. Vertical bars indicate ±1*SEM* (*N* = 10).